



Stochastic response of a tension leg platform to viscous and potential drift forces

Ahsan Kareem

Department of Civil Engineering and Geological Sciences, University of Notre Dame, Notre Dame, Indiana 46556-0767, USA

&

Yousun Li

Shell Development Company, Houston, Texas 77001-0481, USA

The wave drift forces on tension leg platforms (TLP) are contributed by second-order potential and viscous wave load effects, the fluctuations in wave surface elevation and the influence of platform displaced position on the wave excitation. These forces are expressed in terms of in phase and out of phase drift forces. In this study, computationally efficient time domain and frequency domain based schemes are developed to evaluate the TLP response to drift forces. These schemes retain the statistical relationship that exists among these drift forces and the first-order wave forces which is important for the combined response analysis. A parameter study is conducted to delineate the relative significance of different drift forces for several representative sea-states.

1 INTRODUCTION

In addition to the wave forces at the typical wave frequencies in a sea-state, a tension leg platform, due to its compliant behavior in the horizontal plane, experiences slowly varying wave drift forces. These forces originate from various mechanisms involving the nonlinearities of the viscous drag and potential forces, variations in free water surface elevation near TLP columns and the nonlinear feedback of the structural response to the wave loads. The tension leg platform has low natural frequencies in the compliant modes, i.e. motion in the horizontal plane. The wave drift forces at the difference frequencies contribute significantly to the TLP motions in the horizontal plane. In view of the significance of environmental loadings an enhanced response prediction capacity is needed to ensure a useful input to the reliable design of TLPs in deep water. This paper focuses on the computation of wave-induced drift forces and associated platform response utilizing computationally efficient schemes.

Many researchers (e.g. de Boom *et al.*¹) have described the drift forces on a TLP as a result of the

second-order terms in the wave diffraction force. This force is often called potential drift force. Others (Finnigan *et al.*,² Botelho *et al.*,³ Salvensen *et al.*⁴) have focused on the fact that the drag force on the TLP components can cause viscous drift force resulting from the nonlinearity in Morison's drag force formulation.

The treatment of viscous forces has either been limited to time domain analyses (Denise & Heaf⁵) which is straightforward, but computationally inefficient, or in the frequency domain based on the equivalent linearization concept (e.g. Li *et al.*,⁶ Natvig & Pendered⁷). However, the equivalent linearization only provides accurate estimates of the mean square force, but fails to account for the slowly varying viscous forces. This shortcoming can be removed by an equivalent stochastic quadratization scheme. In this approach, the nonlinear viscous force is expressed in terms of a quadratic nonlinearity, e.g. a polynomial up to the quadratic term. This approach retains the important features of the nonlinear interactions and introduces spectral contents at the sum and difference frequencies (e.g. Donley & Spanos,⁸ Kareem & Li,^{9,10} Olagnon *et al.*¹¹ and Zhao & Kareem¹²). Some of these studies utilize the Volterra series or Hermite polynomial expansion to express quadratic nonlinearity. In some of the studies, the structural response is assumed Gaussian or the

response is decomposed into various components to benefit from the Gaussian assumption, while others treat response as a non-Gaussian process by approximating the distribution by a Gram–Charlier type expansion.

McIver¹³ and Rainey¹⁴ reported that the wave effects on TLPs should be evaluated at their displaced position. By neglecting this effect, one may underestimate response results in drift force (Kareem & Li,⁹ Li & Kareem¹⁵ and Spanos & Agarwal¹⁶), which herein is called displacement feedback drift force.

In this study, numerical schemes are developed, in both time and frequency domains, to describe the TLP response induced by different drift forces which is not a simple summation of the individual drift forces discussed above. The statistical relationship among these drift forces and with the first-order wave forces needs to be included in a combination rule.

DRIFT FORCE DESCRIPTION

Potential drift

The potential drift force on a TLP can be described in a manner similar to that for a moored ship (e.g. Pinkster¹⁷). The nonlinearities that appear in the description of diffraction force on a TLP result from the second-order term in the Bernoulli's equation and the wave surface effects. The potential drift can be expressed as

$$\mathbf{F}_{\text{pot}}(t) \stackrel{\text{Re}}{=} \int_{A_0} 1/2 |\nabla \phi(t, \mathbf{r})|^2 \mathbf{T}(\mathbf{r}) dA - \int_{WL} 1/2 \rho g \eta^2(t, \mathbf{r}) \mathbf{T}(\mathbf{r}) dL \quad (1)$$

in which A_0 is the TLP area under mean water level, WL represent the circumference of the submerged component, and $\mathbf{T}(\mathbf{r})$ denotes the transformation from local to platform-fixed coordinates. The wave potential can be expressed as a transformation of the reference wave elevation

$$\begin{aligned} \phi(t, \mathbf{r}) &= \sum_{n=1}^{N_f} H_{\Phi}(f_n, \mathbf{r}) \eta(f_n) \exp j(2\pi f_n t + \epsilon_n) \\ H_{\Phi}(f, \mathbf{r}) &= H_{\Phi_1}(f, \mathbf{r}) + H_{\Phi_s}(f, \mathbf{r}) + j2\pi f_n \mathbf{H}_{\Phi_R}^T(f, \mathbf{r}) \\ &\quad \times \{-(2\pi f_n)^2 [\mathbf{M} + \mathbf{A}(f_n)] + \mathbf{K}\}^{-1} \mathbf{H}_S(f_n) \end{aligned} \quad (2)$$

where $H_{\Phi_1}(f, \mathbf{r})$ and $H_{\Phi_s}(f, \mathbf{r})$ are transfer functions relating $\eta(f)$ to the incident wave potential and scattered wave potential. $\mathbf{H}_{\Phi_R}(f, \mathbf{r})$ is a transfer function vector (6,1) of radiation potential caused by the platform's six-degree-of-freedom oscillations in the six degrees of freedom with unit amplitude. \mathbf{M} , $\mathbf{A}(f_n)$ and \mathbf{K} are offshore structural systems mass, added mass

and stiffness matrices (dimensions: 6,6). $\mathbf{H}_S(f_n)$ is the diffraction force vector (6,1) due to a unit amplitude of regular wave of frequency f_n .

Accordingly, the wave surface elevation near the body becomes a transformation of the reference wave surface elevation,

$$\eta(t, \mathbf{r}) = - \sum_{n=1}^{N_f} \frac{H_{\Phi}(f_n, \mathbf{r})}{g} \eta(f_n) \exp j(2\pi f_n t + \epsilon_n) \quad (3)$$

It is noted that second-order wave potential forces are quadratic transforms of the wave surface elevations (eqns (1), (2) and (3)). By neglecting the high frequency part, the potential drift forces have the following form:

$$\begin{aligned} F_{\text{pot}}(t) &= \sum_{n=1}^{N_f} \sum_{m=1}^{N_f} \mathbf{P}(f_n, f_m) \eta(f_n) \eta(f_m) \\ &\quad \times \cos(2\pi f_{n-m} t + \epsilon_n - \epsilon_m) \\ &\quad + \sum_{n=1}^{N_f} \sum_{m=1}^{N_f} \mathbf{Q}(f_n, f_m) \eta(f_n) \eta(f_m) \\ &\quad \times \sin(2\pi f_{n-m} t + \epsilon_n - \epsilon_m) \\ &= \sum_{n=1}^{N_f} \sum_{m=1}^{N_f} \mathbf{H}_{\text{pot}}(f_n, f_m) \eta(f_n) \eta(f_m) \\ &\quad \times \exp [j(2\pi f_{n-m} t + \epsilon_n - \epsilon_m)] \end{aligned} \quad (4)$$

in which $\mathbf{H}_{\text{pot}}(f_n, f_m)$ is the quadratic transfer function, and $\mathbf{P}(f_n, f_m)$ and $\mathbf{Q}(f_n, f_m)$ are *in-phase* and *out-of-phase transfer functions*, respectively.

$$\mathbf{H}_{\text{pot}}(f_n, f_m) = \mathbf{P}(f_n, f_m) j \mathbf{Q}(f_n, f_m) \quad (5)$$

$\mathbf{H}_{\text{pot}}(f_n, f_m)$ describes the steady drifting forces on a body in an incident monochromatic wave at frequency f_n with a unit amplitude. $\mathbf{H}_{\text{pot}}(f_n, f_m)$ with $n \neq m$, represents the second-order potential forces on the structure at difference frequency (f_{n-m}) when exposed to bi-chromatic waves at frequencies f_n and f_m with unit amplitudes. The real part $\mathbf{P}(f_n, f_m)$ of $\mathbf{H}_{\text{pot}}(f_n, f_m)$ is the potential drift force with the same phase as the envelope of the wave surface elevation and the imaginary part $\mathbf{Q}(f_n, f_m)$ is the drifting force at $\pi/2$ phase difference with respect to the wave surface elevation envelope.

Details concerning the computation of $\mathbf{H}_{\text{pot}}(f_n, f_m)$ used in this study are given in the Appendix. It is important that the diffraction code utilized in the evaluation of $\mathbf{H}_{\text{pot}}(f_n, f_m)$ must include the interactions of different TLP components, e.g. TLP legs. In Fig. 1, a comparison of first-order and second order wave diffraction forces for a typical TLP is given (Kareem & Li⁹). It is noted that the peaks in the drift force description are close to the valleys of the diffraction force and the valleys of the drift force are close to the peak diffraction force. Numerical experiments also suggest that, though not important in the typical

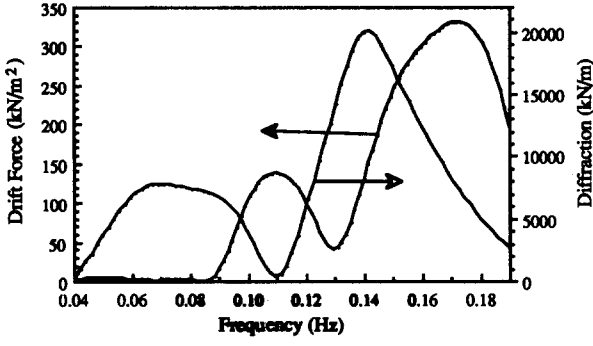


Fig. 1. Diffraction and drift forces.

wave-frequency band, the oscillations of a TLP contribute to the drifting forces at frequencies larger than 0.13 Hz. In the ship motion studies, the out-of-phase force is ignored and the in-phase drift force is approximated by

$$\mathbf{P}(f_n, f_m) \approx \mathbf{P}(f_n, f_n) \quad (6)$$

In Fig. 2a the in-phase drift forces are shown which are close to the steady drift force when Δf is quite small. Most of the TLP has natural frequencies in its horizontal motion around 0.01 Hz. However, the approximation in eqn (6) given by Newman¹⁸ may not be very accurate for TLP analysis since the out-of-phase drift force is more important than the in-phase drift force for small kD where k and D are wave number and column diameter, respectively (Fig. 2b).

The drift force in the time domain is given by

$$\mathbf{f}_{\text{pot}}(t) = \int \int_{-\infty}^{\infty} \mathbf{h}_{\text{pot}}(\tau_1, \tau_2) \eta(t - \tau_1) \eta(t - \tau_2) d\tau_1 d\tau_2 \quad (7)$$

in which $\mathbf{h}_{\text{pot}}(\tau_1, \tau_2)$ is a double Fourier transform of $\mathbf{H}_{\text{pot}}(f_n, f_m)$. In order to reduce computational effort in the evaluation of the preceding equation we introduce the following approximation. The drift force is expressed as a linear transform of the square of the wave surface envelope: $\eta^2(t) + \hat{\eta}^2(t)$, in which $\hat{\eta}(t)$ is the Hilbert transform of $\eta(t)$. This approach can be further simplified by

$$\mathbf{f}_{\text{pot}}(t) \approx \int_{-\infty}^{\infty} \mathbf{h}_{\text{pot}}(\tau) \eta^2(t - \tau) d\tau \quad (8)$$

in which the convolution kernel vector $\mathbf{h}'_{\text{pot}}(t)$ is the Fourier transform of the simplified potential drift force transfer function vector $\mathbf{H}'_{\text{pot}}(\mathbf{f})$. The absolute value of the transfer function vector is given by

$$|\mathbf{H}'_{\text{pot}}(f)|^2 = \frac{\int_0^{\infty} |\mathbf{H}_{\text{pot}}(g+f, g)|^2 G_{\eta}(f+g) G_{\eta}(g) dg}{\int_0^{\infty} G_{\eta}(f+g) G_{\eta}(g) dg} \quad (9)$$

for $f < 0.03$ Hz and smoothly reduces to zero after

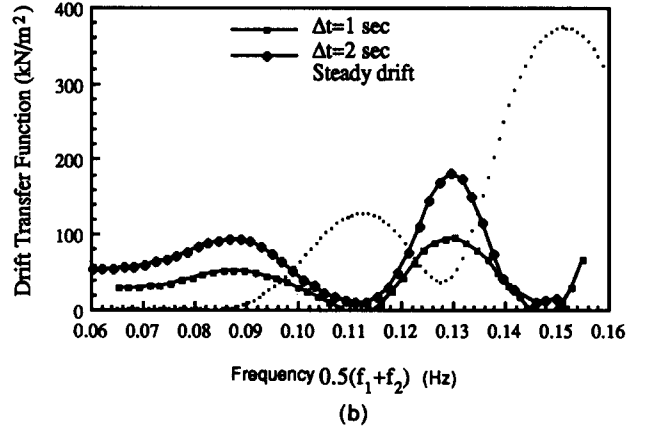
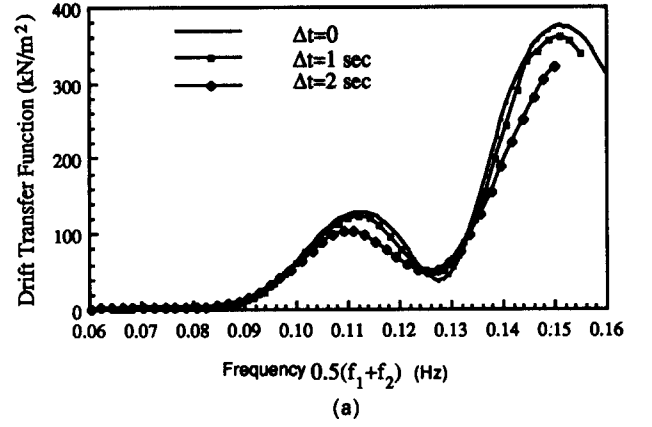


Fig. 2. (a) In-phase surge drift transfer function. (b) Out-of-phase surge drift transfer function.

$f > 0.03$ Hz, and its phase is given by

$$\begin{aligned} & \text{Arg}[\mathbf{H}'_{\text{pot}}(f)] \\ &= \text{Arg} \left\{ \frac{\int_0^{\infty} \mathbf{H}_{\text{pot}}(g+f, g) G_{\eta}(g+f) G_{\eta}(g) dg}{\int_0^{\infty} G_{\eta}(f+g) G_{\eta}(g) dg} \right\} \quad (10) \end{aligned}$$

where $G_{\eta}(f)$ is the two-sided wave height fluctuation spectrum. A continuous function $\mathbf{H}'_{\text{pot}}(f)$ can be obtained by interpolation of computed values of a few discrete frequencies. The simplified transfer function is wave spectrum dependent. Figure 3 shows a simplified transfer function derived from the transfer function shown in Figs 2a and 2b. Accordingly, the derived potential drift force retains correct energy, phase relationship with other drift forces, and the quadratic relationship with wave surface fluctuation. However, based on this approximation, the drift force becomes fully-coherent with the square of the wave surface envelope. Strictly speaking, this may not always be true. Nevertheless, for a narrow banded wave spectrum, the error is not significant. Numerical tests show that normally this coherence function is greater than 0.95 when frequencies are smaller than 0.03 Hz.

The method suggested here, in the time domain,

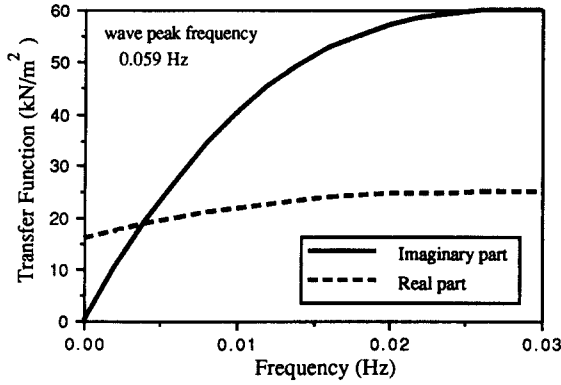


Fig. 3. Simplified transfer function for potential drift forces.

significantly reduces computation effort without compromising accuracy. The spectral density functions estimated from simulated time series of the drifting forces obtained by the proposed method were compared with those derived from the frequency domain based on quadratic transfer function. No discernible differences between the two approaches were found.

Viscous drift

The viscous drift force originates from the nonlinear part of the drag force described by the Morison equation. A statistical quadratization approach is utilized to analyze the effect of nonlinear viscous drag force on platforms (e.g. Kareem & Li,⁹ Li & Kareem¹⁵ and Spanos & Donley¹⁹). This approach improves upon using conventionally utilized statistical linearization approach which fails to bring out energy in the sum and difference frequencies. In this approach, the nonlinearity, e.g. drag force, is expressed by an equivalent polynomial in which up to quadratic terms are included.

In this study, the viscous hydrodynamic loads on TLPs involving nonlinear drag are expressed in terms of multivariate Hermite polynomials correct up to the quadratic term. In this manner the drag force is decomposed in terms of mean, viscous exciting and viscous damping terms (linear) and slowly varying drift force vector is given by

$$\mathbf{f}_{\text{drag}}(\mathbf{x}) = \int_{-L}^{\eta(t)} \frac{1}{2} \rho \mathbf{T}^T(\mathbf{x}) C_d D[\mathbf{u}(t, \mathbf{x}) - \mathbf{T}(\mathbf{x}) \dot{\mathbf{X}}(t)] \times |\mathbf{u}(t, \mathbf{x}) - \mathbf{T}(\mathbf{x}) \dot{\mathbf{X}}| dl \quad (11)$$

where \mathbf{x} is the location vector of a point on the column, \mathbf{X} is the global displacement of the platform, $\mathbf{T}(\mathbf{x})$ is the global to local coordinate transformation matrix, and $\mathbf{u}(t, \mathbf{x})$ is the water particle velocity vector. The part within the bracket in the right-hand side of the preceding equation represents the relative velocities with respect to the body-fixed coordinate system. The total drag force can be separated into two parts, i.e.

below and above the mean water level. There are a number of approaches for evaluating the water particle velocities in the wave crest region. For example, if we use the modified stretch theory, (Mo & Moan²⁰), the water particle velocities in the wave crest are assumed to be uniform with a magnitude equal to that of the mean water level calculated by the linear wave theory. Accordingly, the integral from 0 to $\eta(t)$ is proportional to $\eta(t)v(t)|v(t)|$. This expression always contains second-order polynomial terms regardless of the existence of currents. A tri-variate Hermite polynomial expansion is utilized to carry out an equivalent quadratization in this case (Li & Kareem²¹).

Typically for the evaluation of the viscous wave loads on TLPs, the platform structure is discretized into a number of small segments. The local viscous drag force is computed for each element. The local drag forces are expressed in terms of global wave induced viscous forces. The mean and linear components of drag are not addressed here. The second-order viscous forces (slowly varying viscous drift forces) consist of a second-order force acting on the portion of the structure under the mean water level and the force on the splash zone.

$$\mathbf{F}_{\text{vis}}^{[2]}(t) = \mathbf{F}_d^{[2]}(t) + \mathbf{F}_{de}^{[2]}(t) \quad (12)$$

$$\mathbf{F}_{\text{vis}}^{[2]}(t) = \sum_{n=1}^{N_e} \mathbf{T}_n \mathbf{C}_n^{[2]}(C_{v_n}) \mathbf{w}^{[2]}(t) + \sum_{n=1}^{N_e} \mathbf{T}_n \mathbf{C}_{\eta_n}^{[2]}(C_{v\eta_n}) \mathbf{w}_{\eta}^{[2]}(t) \quad (13)$$

in which the quadratic (second-order) matrix at the n th element, $\mathbf{C}_n^{[2]}$ and $\mathbf{C}_{\eta_n}^{[2]}$, can be found in Li & Kareem²² and $\mathbf{w}^{[2]}(t)$ and $\mathbf{w}_{\eta}^{[2]}(t)$ are the quadratic components of the relative fluid-structure velocity (Li & Kareem²¹).

3 DRIFT FORCES INTRODUCED BY DISPLACED POSITION

The wave forces computed at the displaced position of offshore structures may introduce additional drift forces. This contribution is particularly significant for compliant offshore structures that are configured by design to experience large excursions under the environmental load effects, e.g. tension leg platforms. In random seas, this feature can be included in the time domain analysis by synthesizing drag and diffraction forces through a summation of a large number of harmonics with an appropriate phase relationship that reflects the platform displaced position. This approach is not only limited to the time domain analysis, but the superposition of a large number of trigonometric terms in such an analysis demands a significant computational effort.

Typically, the wave kinematics and diffraction forces

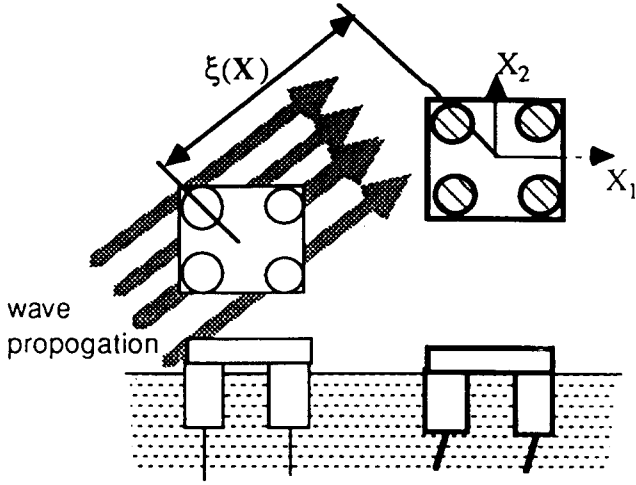


Fig. 4. Schematic description of TLP displacement.

are described in terms of a linear transform of the reference wave-surface elevation. For example,

$$\mathbf{F}_s(t) = \int_{-\infty}^{\infty} \mathbf{H}_s(f) \eta(f) \exp(j2\pi ft) df \quad (14)$$

in which $\mathbf{H}_s(f)$ is the transfer function vector that relates the wave-surface elevation and the diffraction forces, and $\eta(f)$ is the Fourier transform of the wave surface elevation $\eta(t)$ at the origin of the space-fixed reference frame. The diffraction force acting on a platform undergoing a displacement $\mathbf{X}(t)$ is given by

$$\mathbf{F}_s(t, \xi(\mathbf{X})) = \int_{-\infty}^{\infty} \mathbf{H}_s(f) \eta(f, \xi(\mathbf{X})) \exp(j2\pi ft) df$$

$$\eta(f, \xi(\mathbf{X})) = \eta(f) \exp[-jk\xi(\mathbf{X})] \quad (15)$$

where k is the wave number and $\xi(\mathbf{X})$ is the instantaneous location of the platform center in the direction of wave propagation (Fig. 4). The preceding equation in the frequency domain is given by

$$F_s(f, \xi(\mathbf{X})) = F_s(f, 0) \exp(-jk\xi(\mathbf{X})) \quad (16)$$

in which $F_s(f, 0)$ are the diffraction forces computed at the undisplaced position.

For the computation of the viscous drag force on a platform the relative fluid-structure velocity is needed at the instantaneous displaced position

$$\mathbf{u}(f, \xi(\mathbf{x})) = \mathbf{u}(f) \exp[-jk\xi(\mathbf{x})] \quad (17)$$

where \mathbf{x} denotes local displacement of a given position on the platform.

The computation of diffraction viscous forces can be facilitated by a feedback scheme. First, the forces at the displaced position are expanded in a Taylor's series about the undisplaced position. This is subsequently expressed in terms of the following format

$$\mathbf{f}(t, \mathbf{x}) = \mathbf{f}^{[1]}(t) + \sum_{i=1}^{\infty} \boldsymbol{\theta}^{[i]}(t) \xi^i(t) \quad (18)$$

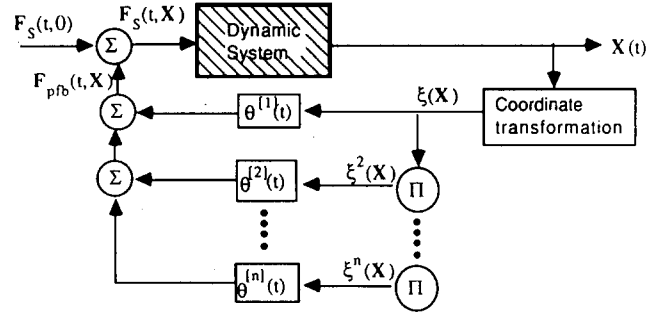


Fig. 5. Displacement induced feedback force.

in which $\boldsymbol{\theta}^{[i]}(t)$ denotes the time-variant feedback coefficient vector which is a linear transform of $\mathbf{f}^{[i]}(t)$, and $\xi(t)$ is the platform displacement along the wave propagation (Li & Kareem¹⁵). The feedback coefficients are given as

$$\boldsymbol{\theta}^{[1]}(t) = \int_{-\infty}^{\infty} -2 \left(\int_0^{\infty} \frac{(2\pi f)^2}{g} \sin(2\pi f \tau) df \right) \times \mathbf{f}^{[1]}(t - \tau) d\tau$$

and

$$\boldsymbol{\theta}^{[2]}(t) = \int_{-\infty}^{\infty} \left(\int_0^{\infty} -\frac{(2\pi f)^4}{g} \cos(2\pi f \tau) df \right) \times \mathbf{f}^{[1]}(t - \tau) d\tau \quad (19)$$

The main contribution of the feedback is an extra drift force due to both potential (diffraction related) and viscous (drag related) effects. In Fig. 5, a schematic representation of a nonlinear displacement feedback system for diffraction force is shown. Details concerning computational procedures for the implementation of the feedback concept are available in Li & Kareem.¹⁵

Before moving to the section on computation methods, we summarize all the drift forces discussed here in Table 1.

Table 1. Anatomy of drift forces

Hydrodynamic origin	Low frequency drift		
	Second order terms	Fluctuation in wave surface elevation	Feedback due to displaced position of platform
Potential-Bernoulli's equation	✓	✓	✓
Viscous—Morrison's drag term	✓	✓	✓

COMPUTATIONAL METHODS

Time domain simulation

The time histories of a random wave field are often simulated as a summation of a number of trigonometric functions (Li & Kareem,²² Shinozuka²³). By utilizing this approach, the energy of the wave field is only contained at a number of discrete frequencies. The second-order processes, e.g. drift, may not be accurately modeled by this approach unless it is based on a very large number of summation terms. The parametric models offer an ideal scheme for simulating time series with continuous energy over the entire spectrum of frequencies of interest. In this approach, the time series of wave surface elevation are first generated by filtering a white noise through a prescribed filter (e.g. Spanos & Mignolet²⁴ and Li & Kareem²⁵). This is followed by linear or nonlinear transformations, which provide simulated wave loads and drift loads (Li & Kareem²⁵).

The potential drift force can be simulated by either utilizing eqn (7) or (8). The latter involves a single convolution; thus it is computationally more efficient than the former. Details concerning the computation of the preceding convolutions can be found in Li & Kareem.²⁵ The computation of viscous drift force follows from eqn (13). The displacement feedback drift forces are based on the procedure that first simulates first-order loads without including the displaced position of the platform. The feedback terms of both potential and viscous origins are then included to compute forces at the displaced position. The digital filters designed to model discrete differentiation and convolution and their hybrid combination are used to evaluate the displacement feedback time-variant coefficients (eqs (18) and (19)). Details are given in Li & Kareem.²⁵

Frequency domain analysis

The frequency domain analysis is primarily used for a linear or quasi-linear system. However, the application of frequency domain schemes can be extended to quadratic or even high-order systems (Kareem & Li¹⁰). In the following, a procedure that facilitates computation of the drift forces in the frequency domain is outlined.

(1) Viscous drift force

The nonlinear drag force can be expanded into a polynomial by statistical error minimization (e.g. Borgman²⁶ and Li & Kareem²¹). The drag force on the immersed part of the column can be expressed as

$$\mathbf{v}(t)|\mathbf{v}(t)| = \mathbf{C}_0 + \mathbf{C}_1\mathbf{v}(t) + \mathbf{C}_2\mathbf{v}^2(t) + \dots \quad (20)$$

In which \mathbf{C}_0 , \mathbf{C}_1 , \mathbf{C}_2 , etc., are the coefficient matrices that depend on the covariance of $\mathbf{v}(t)$, the relative

fluid–structure velocity, and $\mathbf{v}^2(t)$ is a vector containing product of the relative velocity components in the local coordinate system, i.e. $\mathbf{v}^2(t) = [v_1^2(t), v_2^2(t), v_1(t)v_2(t)]^T$. The drag force due to the wave profile above the mean water level is given by

$$\mathbf{v}(t)|\mathbf{v}(t)|\eta(t) = \mathbf{D}_0 + \mathbf{D}_1\mathbf{v}(t) + \mathbf{D}_2\mathbf{v}(t)\eta(t) + \dots \quad (21)$$

in which \mathbf{D}_0 , \mathbf{D}_1 , \mathbf{D}_2 , etc., are coefficient matrices that are functions of the covariance of $\mathbf{v}(t)$ and $\eta(t)$. All of these quadratic terms are viscous drift forces, their spectral density function can be computed by a spectral convolution approach (Brigham²⁷).

(2) Potential drift force

The potential drift force spectrum can be evaluated from the quadratic transfer function by the following

$$\mathbf{G}_{\text{pot}}(f) = 8 \int_0^\infty |H_{\text{pot}}(f_1 + f, f_1)|^2 \times G_\eta(f_1)G_\eta(f + f_1) df_1 \quad (23)$$

in which $G_\eta(\cdot)$ represents single sided wave height spectrum.

(3) Feedback drift force

Let the reference origin be at the center of the platform at its mean offset position. The feedback terms given by a summation in the right-hand side of eqn (18) may be truncated and the first term is given by

$$\mathbf{f}_{\text{fdbk}}(t) = \theta^{[1]}(t)\xi(t) \quad (23)$$

in which $\mathbf{f}_{\text{fdbk}}(t)$ is the feedback drift force vector. Its spectral density function can be computed by a spectral convolution approach involving the spectra of the first-order wave loads and the response (Li & Kareem²²).

The computation of the viscous and feedback drift forces in the frequency domain involves the contribution of platform response. This poses additional computational difficulty, which can be overcome by using an iteration technique, a perturbation technique, or a combination of these, Kareem & Li.⁹ Typically, the viscous force is evaluated by a summation of the viscous drift force on discretized components of the TLP. The spectral density function of a process resulting from the summation of a number of processes involves the spectra and cross-spectra of these respective processes. For unidirectional linear waves, the computation of the cross-spectral density functions can be eliminated by introducing a complex Fourier amplitude concept.

Let us define the complex Fourier amplitude of the water surface elevation as

$$\hat{\eta}(f_n) = \sqrt{G_\eta(f_n)\Delta f} \quad (24)$$

in which $f_n = n\Delta f$ and $G_\eta(f_n)$ is the single-sided spectrum of the wave surface elevation. Then all first-order wave processes can be expressed in terms of the complex Fourier amplitude. Its amplitude is related to

the spectrum and its argument is the phase with respect to the wave surface elevation at the reference location. The linear transformation becomes a simple operation, for example, the wave velocity vector at a location \mathbf{x} is given by

$$\hat{\mathbf{u}}(f_n, \mathbf{x}) = \mathbf{H}_u(f_n, \mathbf{x})\hat{\eta}(f_n) \quad (25)$$

in which $\mathbf{H}_u(f_n, \mathbf{x})$ is the transfer function. The first-order wave load can be computed in terms of the complex Fourier amplitude, $\hat{\mathbf{f}}^{[1]}(f_n)$. Accordingly, the first-order response vector becomes

$$\hat{\mathbf{X}}^{[1]}(f_n) = \mathbf{H}_{\text{sys}}(f_n)\hat{\mathbf{f}}^{[1]}(f_n) \quad (26)$$

The spectral density matrix of the response in terms of the six degrees of freedom is given by

$$\mathbf{G}_{\mathbf{x}}^{[1]}(f_n) = \frac{\sum_{n=0}^{n_{\text{max}}} \hat{\mathbf{X}}^{[1]}(f_n)\hat{\mathbf{X}}^{[1]*}(f_n)}{\Delta f} \quad (27)$$

As for the drift forces, which are the quadratic transformations of the first order wave field, the complex Fourier amplitudes are expressed as functions of two frequencies. The potential drift force based on eqns (7) and (8) is given by

$$\hat{\mathbf{f}}_{\text{pot}}(f_n, f_{n+p}) = \mathbf{H}_{\text{pot}}(f_n, f_{n+p})\hat{\eta}(f_n)\hat{\eta}^*(f_{n+p}) \quad (28)$$

or

$$\hat{\mathbf{f}}_{\text{pot}}(f_n, f_{n+p}) \approx \mathbf{H}'_{\text{pot}}(f_p)\hat{\eta}(f_n)\hat{\eta}^*(f_{n+p}) \quad (29)$$

The viscous drift force is expressed as

$$\mathbf{f}_{\text{vis}}(f_n, f_{n+p}) = \sum_{r=1}^N \mathbf{T}^T(\mathbf{X}_r)\mathbf{C}_2 \left\{ \begin{array}{l} 2 \text{Re} [\hat{v}_1(f_n, \mathbf{x}_r)\hat{v}_1^*(f_{n+p}, \mathbf{x}_r)] \\ 2 \text{Re} [\hat{v}_2(f_n, \mathbf{x}_r)\hat{v}_2^*(f_{n+p}, \mathbf{x}_r)] \\ \hat{v}_1(f_n, \mathbf{x}_r)\hat{v}_2^*(f_{n+p}, \mathbf{x}_r) + \hat{v}_2(f_n, \mathbf{x}_r)\hat{v}_1^*(f_{n+p}, \mathbf{x}_r) \end{array} \right\} \quad (30)$$

and the feedback drift force is expressed as

$$\hat{\mathbf{f}}_{\text{fdbk}}(f_n, f_{n+p}) = \hat{\boldsymbol{\theta}}(f_n)\hat{\xi}^*(f_{n+p}) + \hat{\xi}(f_n)\hat{\boldsymbol{\theta}}^*(f_{n+p}) \quad (31)$$

The complex Fourier amplitude vector of the total drift force is now a simple summation of those for all the drift forces:

$$\hat{\mathbf{f}}^{[2]}(f_n, f_{n+p}) = \hat{\mathbf{f}}_{\text{pot}}(f_n, f_{n+p}) + \hat{\mathbf{f}}_{\text{vis}}(f_n, f_{n+p}) + \hat{\mathbf{f}}_{\text{fdbk}}(f_n, f_{n+p}) \quad (32)$$

The drift-induced response vector is given by

$$\hat{\mathbf{X}}^{[2]}(f_n, f_{n+p}) = \mathbf{H}_{\text{sys}}(f_p)\hat{\mathbf{f}}^{[2]}(f_n, f_{n+p}) \quad (33)$$

Table 2. Basic characteristics of example

Column diameter	18.06 m
Column draft	13.9 m
Column span	66.22 m
Pontoon diameter	9.03 m
Tether stiffness	18925 kN/m \times 4 each column
Tether pretension	10200 kN \times 4 each column
Mass center of the platform	6.02 m above mean water level
Mass	2.8×10^7 kg
Inertial moment	3×10^{10} kg m ² (w.r.t. MWL)

Finally, the spectral matrix of the response is given by

$$\mathbf{G}_{\mathbf{x}}^{[2]}(f_p) = \frac{\sum_{n=0}^{n_{\text{max}}} \hat{\mathbf{X}}^{[2]}(f_n, f_{n+p})\hat{\mathbf{X}}^{[2]*}(f_n, f_{n+p})}{2\Delta f} \quad (34)$$

5 EXAMPLE

The relative significance of different types of drift forces on the TLP response was assessed in this study. A generic, symmetrical TLP configuration was utilized for this study. Important geometric and structural features of the TLP are given in Table 2.

In view of the quadratic relation between the drift-induced response and the wave surface elevation, the following *drift response ratios* are introduced:

$$\chi_{\bar{D}}(f_o) = \frac{\sigma_{X_1}(f_o)}{\sigma_{\eta}^2(f_o)} \quad (35)$$

$$\chi_{\bar{D}}(f_o) = \frac{\bar{X}_1}{\sigma_{\eta}^2}$$

where $\chi_{\bar{D}}(f_o)$ and $\chi_{\bar{D}}(f_o)$ denote the response ratios as functions of f_o , \bar{X}_1 denotes the mean offset induced by the drift force, and $\sigma_{X_1}(f_o)$ and $\sigma_{\eta}(f_o)$ are the standard deviations of the response and the wave surface elevation of the peak frequency f_o . The concept developed herein is useful in comparing the contributions of the various drift force to the response and also a convenient way to make preliminary estimation of the response induced by several components of the drift forces.

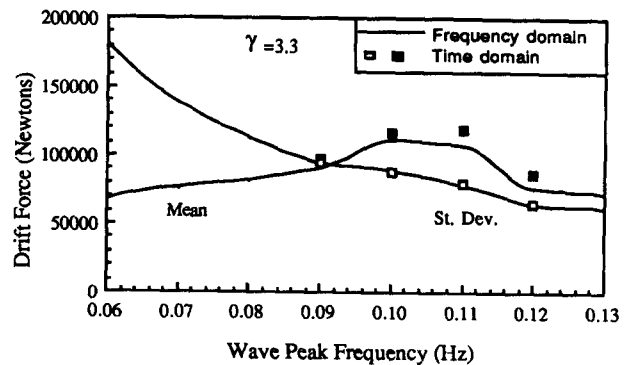


Fig. 6. Potential drift force in surge.

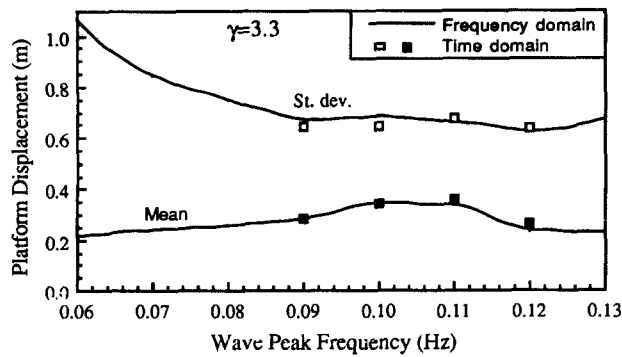


Fig. 7. Surge response to potential drift force.

Potential drift

Figures 6–8 highlight the potential drift force, the corresponding platform response and the ratio of the response to the variance of the wave surface elevation, respectively. It is noted in Fig. 8 that the ratio of the response to wave height rapidly increases with an increase in the wave peak frequency.

Salvensen *et al.*⁴ utilized a deterministic wave of period of 9.5 seconds to demonstrate that in an extreme sea state the steady surge due to wave drift (mainly potential drift) is more important than any of the other forces, e.g. winds, currents and wave diffraction forces. The significance of the potential drift force for random waves is demonstrated here. Let us consider the JONSWAP spectrum with the wave peak frequency $f_o = 0.11$ Hz, $\gamma = 6.89$ and $\alpha = 0.0485$ (Spidsoe & Sigbjornsson²⁸). The platform response spectral density functions are plotted in Fig. 9. The mean and standard deviation of the response are listed in Table 3. The platform mean offset due to the potential drift force is equivalent to that induced by 0.8 m/s currents (Kareem & Li⁹). The response at wave-frequency is negligible in comparison with the response due to drift, and the standard deviation of the response due to the wave drift alone is equivalent to that due to 20 m/s winds (Kareem & Li⁹).

In Figs 6, 7 and 9 and Table 3 it is demonstrated that the results obtained by the time and frequency domains

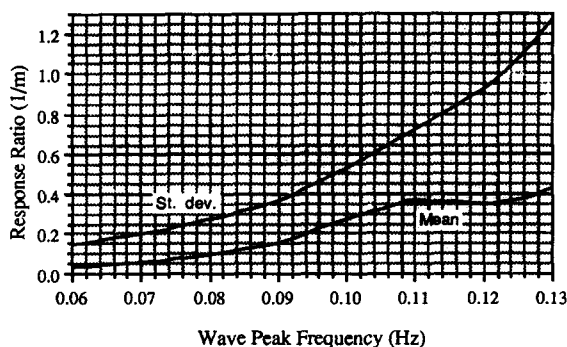


Fig. 8. Surge response ratio due to potential drift.

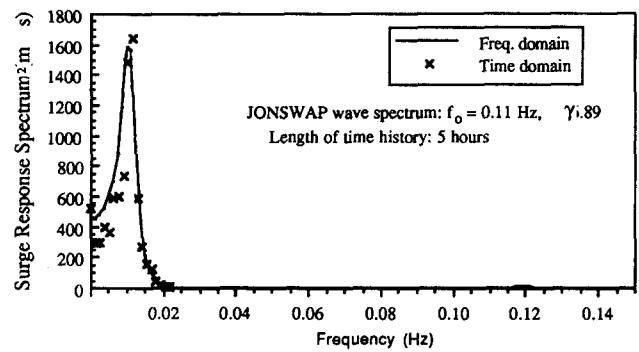


Fig. 9. Spectral density function of surge drift response.

are very close, and the approximate method tends to overestimate everything except for the mean component since some of the nonlinear interactions are neglected in this approach.

Viscous drift

As stated earlier the viscous drift force consists of two sources: the second-order term of Morison drag force acting on the structure below the mean water level and the drag force acting on the splash zone due to the variations in the wave surface elevation above the mean water level. The viscous drift force below the mean water level is only possible in the presence of currents.

The wave-induced viscous forces on the splash zone with and without currents corresponding to different waves are presented in Fig. 10. It is noted in this figure that the force (only in the order of 10^4 newtons) is much smaller than the force on the splash zone when the platform is assumed to be fixed. The viscous force on the splash zone largely depends on the correlation between the wave surface elevation and the relative fluid-structure velocities. In these examples, the water particle velocities and the platform velocity response have nearly the same phases and amplitudes, which result in the normalized correlation between the relative velocity and wave surface elevation on the order of 5%. Hence, both the steady and fluctuating components of this viscous force appear to be of little significance. These examples are based on the JONSWAP spectrum with an average peak ratio (i.e. $\gamma = 3.3$). However, in some extreme cases, this force can be more significant, an example of which will be given later. It is also noted in this figure that the force on the splash zone is enhanced by the presence of currents.

The TLP response at low frequencies is only caused

Table 3. Response computed by different methods (conditions: Fig. 9, $\sigma_w = 2.926$ m)

Item	Time domain	Frequency domain	Approximate
Mean offset	3.00 m	3.07 m	3.08 m
St. dev. (< 0.02 Hz)	3.18 m	3.54 m	6.16 m
St. dev. (> 0.02 Hz)	0.605 m	0.534 m	0.70 m

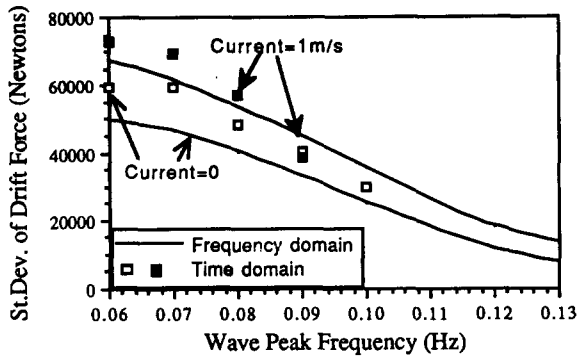


Fig. 10. Viscous drift force on the splash zone.

by the viscous drift force acting on the splash zone in the absence of the currents (Fig. 11). It is noted that the standard deviations computed in the frequency and time domains are not very close. Since the value of the drift force is small, various numerical errors may become significant enough to cause some discrepancies in the forces and response obtained in the time and frequency domains (Figs 10 and 11).

In Fig. 12, the contribution of currents is included. The mean offset of the platform in this case is caused by a combined effect of the currents and waves. Both the mean and the standard deviation of the response show good agreement between the results in the time and frequency domains.

The results in Figs 10–12 suggest that the viscous drift force and the corresponding displacement response decrease with an increase in the wave peak frequency. This is attributed to the lack of kinetic energy associated with the waves at high wave peak frequencies described by the JONSWAP wave spectrum.

The results in Fig. 13 provide the response ratios in the presence and absence of currents. It is noted in this figure that the response ratio to the wave surface elevation rapidly increases with an increase in the wave peak frequency until $f_0 = 0.1$ Hz and subsequently approaches a plateau. A similar trend has been reported by Finnigan *et al.*²

Let us examine an extreme sea state with large waves, assuming that the wave peak frequency is equal to 0.09 Hz and the wave parameters are $\gamma = 6$ and $\alpha = 0.0202$ (Spidsoe & Sigbjornsson).²⁸ This input

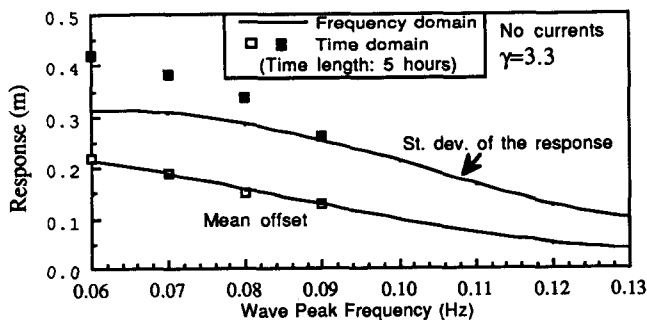


Fig. 11. Surge drift due to wave viscous forces.

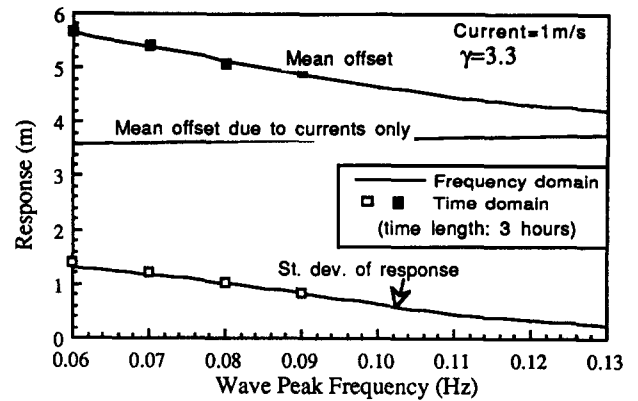


Fig. 12. Surge drift due to viscous forces.

information provides the standard deviation of the wave surface elevation equal to 2.765 m. The spectral density functions of the response in the absence and presence of currents shown in Figs 14(a) and 14(b) illustrate that the low frequency motion induced by the viscous drift force is larger than the wave-frequency response. The oscillatory response in the absence of currents (due to the viscous force on the splash zone) could still be quite large in this case (Fig. 14(a)). The spectral density functions obtained by the frequency and time domains provide a good agreement. The unsmoothed estimates of the spectral density function derived from the time history of the response are inherently oscillatory (Bendat & Piersol²⁹). Therefore, to provide a better comparison, the standard deviation of the response based on the three methods (time domain, frequency domain, and approximate method based on response ratio) is compared in Table 4. The results also include motions in other compliant modes, i.e. sway and yaw. It is noted that the results from the time and frequency domains are in perfect agreement and that the concept of the normalized wave-frequency response and the drift ratio offer an approximate prediction of the response with an error of less than 10%, except for the mean offset of the platform in the absence of currents which has a very small value. It is also noted in Table 4 that the interactions introduced by

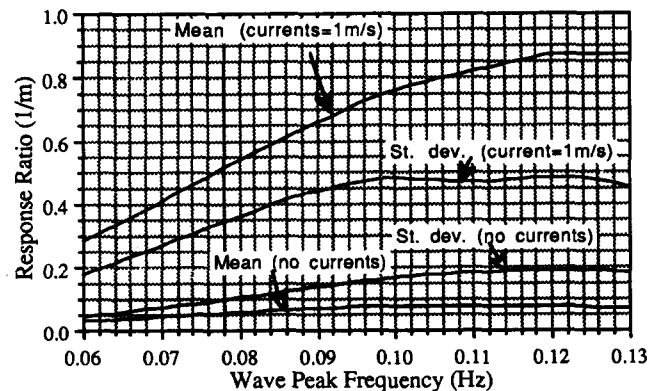
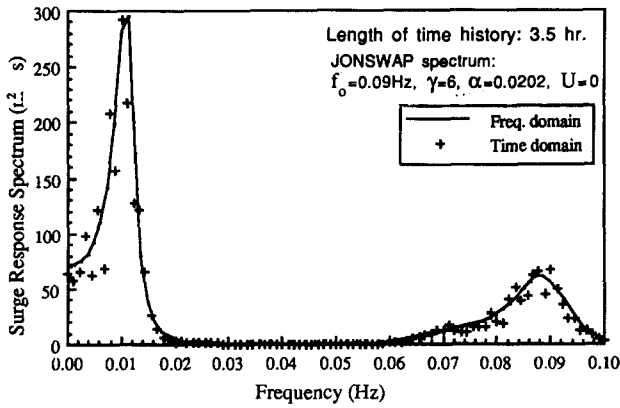


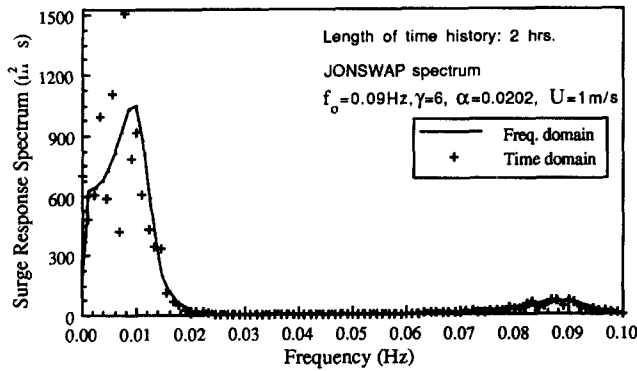
Fig. 13. Surge drift ratio.

Table 4. Response computed by different methods (conditions: Fig. 14(a) and (b), $\sigma_y = 2.76$ m)

	Item		Time domain	Frequency domain	Approximate
$U = 1.4$ m/s at 45° angle of approach	Surge (m)	Mean	8.900	8.66	8.5
		St. dev. (≤ 0.023 Hz)	2.931	3.027	3.13
		St. dev. (> 0.023 Hz)	1.072	1.030	0.97
	Sway (m)	Mean	6.066	5.97	—
		St. dev. (≤ 0.023 Hz)	0.586	0.527	—
Yaw (rad)	Mean	0.000726	0.000801	—	
	St. dev. (< 0.023 Hz)	0.00101	0.00108	—	
$U = 0$	Surge (m)	Mean	0.9383	0.964	0.53
		St. dev. (≤ 0.023 Hz)	1.399	1.470	1.35
		St. dev. (> 0.023 Hz)	0.988	1.020	0.97



(a)



(b)

Fig. 14. (a) Spectral density function of surge response. (b) Spectral density function of surge response w/current.

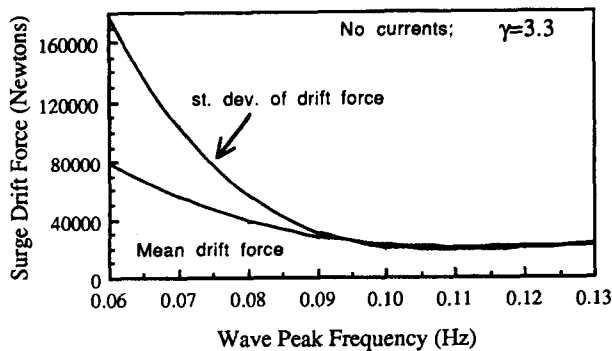


Fig. 15. Mean displacement feedback forces in surge.

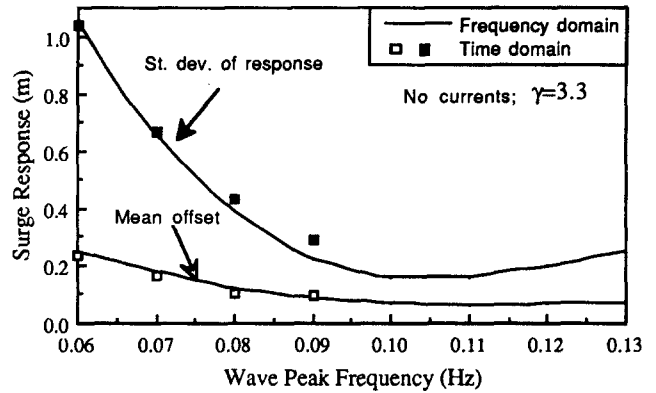


Fig. 16. Surge drift due to displacement feedback.

the nonlinearity in the drag force terms of the water particle velocity vector result in sway and yaw motions for wave propagation at zero angle of incidence when currents approach at 45° angle of attack.

Displacement-induced feedback drift

For the example under consideration, the mean and standard deviation of the force and corresponding response due to the displacement feedback are presented in Figs 15 and 16. In the time domain it is not convenient to delineate the feedback force from the

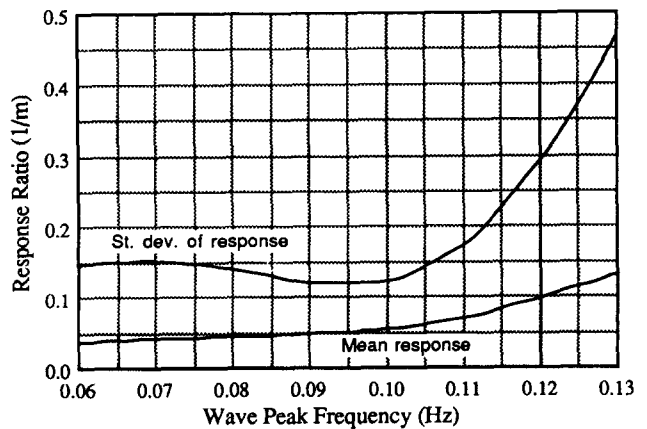


Fig. 17. Response ratio due to displacement feedback.

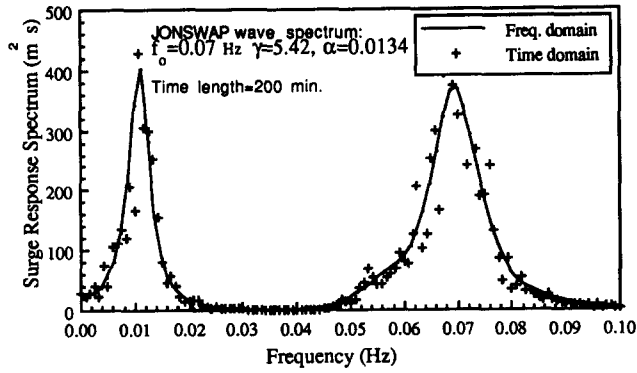


Fig. 18. Spectral density function of surge response due to feedback.

others, therefore, in Fig. 15 only the frequency domain values are plotted. The ratio of the response to the variance of the wave surface elevation is shown in Fig. 17. These figures demonstrate that the oscillatory component due to the displacement feedback is more significant in comparison with the mean offset. The results given in Fig. 16 suggest that the response due to the feedback is significant only for the sea state described by the low wave peak frequencies.

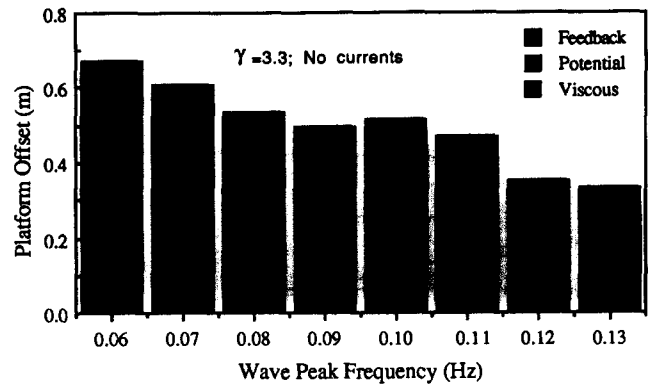
The response spectrum in an extreme sea state is presented in Fig. 18 and Table 5. The spectral description demonstrates that the response due to displacement feedback is only slightly smaller than the wave-frequency response. As noted in the previous examples, the frequency domain response provides good agreement with the time domain results. The approximate procedure provides higher values.

Summary of the wave-induced drift effects

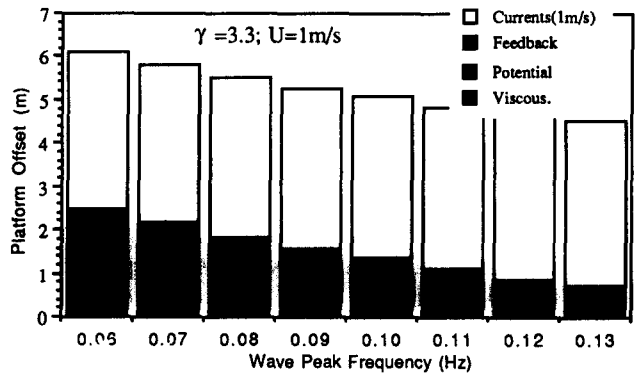
In this section, the relative contribution of TLP response due to different drift forces is delineated. In Figs 19a and 19b the mean offset of the platform under different drift forces with or without currents is presented. These figures suggest that in general all three mechanisms contribute to the platform mean offset in the absence of currents. In contrast, the currents and the viscous drift effects have a major contribution in the presence of currents. Figure 20 presents the standard deviation of the slowly varying surge motion under different wave drift forces. The contribution of the viscous drift force is relatively insignificant in the absence of currents, but the addition of currents in combination with the waves of

Table 5. Response computed by different methods (conditions: Fig. 18, $\sigma_\eta = 3.7$ m)

Item	Time domain	Frequency domain	Approximate
Mean offset	0.560 m	0.637 m	0.640 m
St. dev. (< 0.02 Hz)	1.54 m	1.57 m	2.10 m
St. dev. (> 0.02 Hz)	2.32 m	2.30 m	2.22 m



(a)



(b)

Fig. 19. (a) Platform mean surge offset due to drift forces. (b) Platform mean offset in surge due to drift forces.

low peak frequencies (less than 0.1 Hz) significantly enhances the contribution of the viscous effects. The potential drift force becomes relatively important only when the wave peak frequency is larger than 0.09 Hz. As noted earlier, the feedback force contributes more in the waves of low peak frequencies.

In Fig. 21, the mean offset and the standard deviation due to all the drift forces (in the presence and absence of currents) are presented. An approximate estimation of the mean offset of the platform can be made by a simple summation of the mean offsets induced by these individual drift forces (compare Figs 19a and 19b with

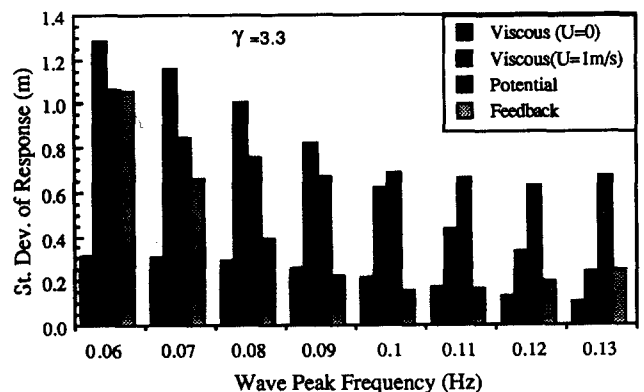


Fig. 20. Comparison of drift force contributions in surge.

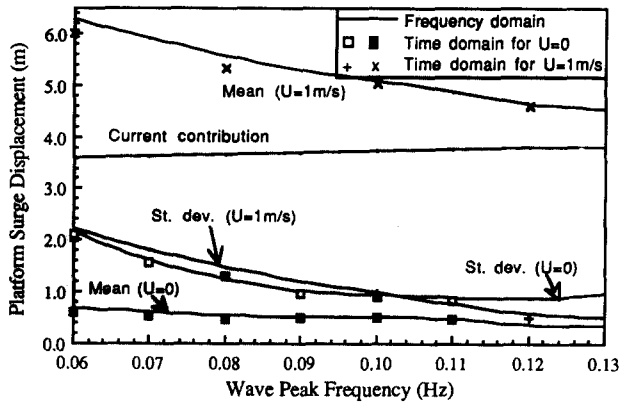


Fig. 21. Platform surge displacement due to drift forces.

Fig. 21). However, it is not possible to add the standard deviation of response contributions from different sources in Fig. 20 because of the correlations that exist among those that range from -1 to $+1$ as well as the nonlinear interactions. (Compare the sum of each contribution in Fig. 20 with Fig. 21.) The combined analysis presented here takes into account the correct correlation that exists among various components. A simple superposition fails to provide accurate results. It is noted in Fig. 21 that the introduction of currents may have positive and negative effects on the response since the currents can induce both the slowly varying drift forces and the viscous damping to excite and suppress the platform oscillations at the same time. The ratio of the response to the variance of the wave surface elevation is given in Fig. 22 for approximate estimation.

A final example concerning the extreme sea state is presented in which $f_0 = 0.09$ Hz, $\gamma = 6$ and $\alpha = 0.0202$ in the presence of 1 m/s currents. It is noted in Fig. 20 that both the potential and the viscous drifts for $f_0 = 0.09$ Hz are important. The spectral density functions are plotted in Fig. 23 and the corresponding data are listed in Table 6. It is noted in the figure and the table that the low frequency response is much greater than the wave-frequency response in this extreme sea state. The results obtained from both the time and frequency domains and from the approximate method are in good agreement.

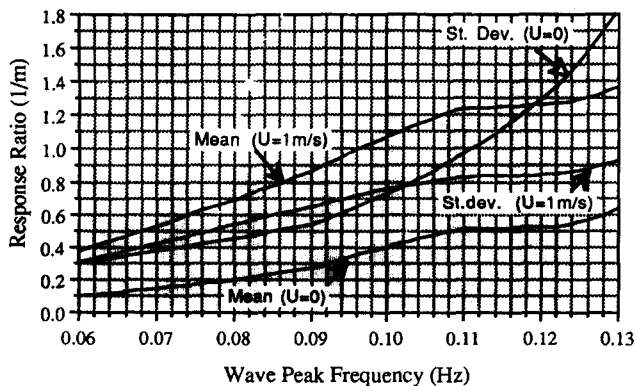


Fig. 22. Drift response ratio.

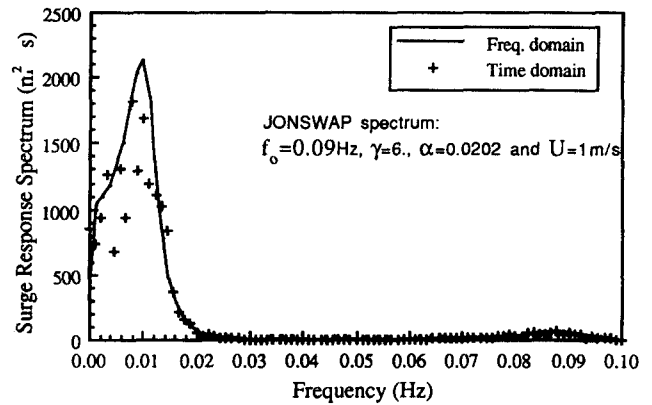


Fig. 23. Spectral density function of surge response.

6 CONCLUSIONS

The drift forces acting on a TLP are categorized here as the potential, viscous and displacement feedback drift forces. These forces originate from various mechanisms involving the nonlinearity in the viscous drag term, nonlinearity in the potential forces, wave free surface variation and the platform displacement. All the drift forces contribute significantly to the TLP motion in the horizontal plane. The parameter study conducted for the example TLP suggests that each of the three drift force mechanisms contribute to the platform mean offset in the absence of currents. TLP response due to viscous drift forces is relatively small in the absence of currents, but the addition of currents in combination with the wave field characterized by peak frequency less than 0.1 Hz enhances the response. The potential drift becomes relatively more predominant for waves with peak frequencies greater than 0.09 Hz. The displacement feedback drift forces contribute more in the waves of low peak frequencies. The total mean offset is a simple summation of the individual components. The same is not valid for the fluctuating drift as the correlation between different sources of drift become important, and a simple superposition yields inaccurate results. In this paper, analysis based on computationally efficient schemes in both the time and frequency domains that take into account the correlation structure among these drift forces in computing the platform response are shown to have a good agreement. It is important to note that additional drift forces that may result from second-order diffraction of waves by the TLP have not been addressed here.

Table 6. Response computed by different methods (conditions: Fig. 23, $\sigma_\eta = 2.76$ m)

Item	Time domain	Frequency domain	Rough estimation
Mean	9.59 m	9.06 m	10.35 m
St. dev. (< 0.03 Hz)	4.26 m	4.65 m	4.97 m
St. dev. (> 0.03 Hz)	1.07 m	1.02 m	0.97 m

ACKNOWLEDGEMENTS

This research was supported by the National Science Foundation under Grant No. CES 8352223 (BCS-90-96274) and matching funds provided by a number of oil companies. The first author would also like to acknowledge the partial support of the Offshore Technology Research Center, NSF Engineering Research Centers Program Grant No. CDR-8721512, during the writing of this manuscript. Any opinions and findings expressed in this presentation are those of the authors and do not necessarily reflect the views of the sponsors or employers.

REFERENCES

- de Boom, W.C., Pinkster, J.A. & Tan, P.S.G., Motion and Tether Force Prediction for a TLP. *Journal of Waterway, Port, Coastal and Ocean Engineering, ASCE*, **110** (1985) 472–86.
- Finnigan, T.D., Petruskas, C. & Bothelho, D.L.R., Time-Domain Model for TLP Surge Response in Extreme Sea States. *Proceeding of the Offshore Technology Conference*, Houston, Tx. OTC 4657, 1984.
- Botelho, D.L.R., Finnigan, T.D., Petruskas, C. & Liu, S.V., Model Test Evaluation of a Frequency-Domain Procedure for Extreme Surge Response Prediction of Tension Leg Platform. OTC 4658, 1984.
- Salvensen, N., von Kerczek, C.H., Yue, D.K. & Stern, F., Computation of Nonlinear Surge Motion of Tension Leg Platforms. OTC 4394, 1982.
- Denise, J-P.F. & Heaf, N.J., A Comparison Between Linear and Nonlinear Response of a Proposed Tension Leg Platform. *Proceedings of the 11th Annual Offshore Technology Conference*, Houston, TX. OTC 3555, 1984.
- Li, Y., Kareem, A. & Williams, A.N., Dynamic Response of a Tension-Leg Platform to Random Wind & Wave Fields. *Proceedings of the Fifth U.S. National Conference on Wind Engineering*, Wind Engineering Research Council, Lubbock, TX, 1985.
- Natvig, B.J. & Pendered, J.W., Nonlinear Motion Response of Floating Structures to Wave Excitation. *Proceedings of the 9th Annual Offshore Technology Conference*, Houston, TX. OTC 2796, 1977.
- Donley, M.G. & Spanos, P.D., Stochastic Response of a Tension Leg Platform to Viscous Drift Forces. *Journal of Offshore Mechanics and Arctic Engineering, ASME*, **113** (1991) 148–55.
- Kareem, A. & Li, Y., Stochastic Response of a Tension Leg Platforms to Wind and Wave. Department of Civil Engineering Technical Report No. UHCE 88-18, University of Houston, 1988.
- Kareem, A. & Li, Y., Equivalent Statistical Quadraticization of Nonlinear Hydrodynamic Loads on TLPs. *Proceedings of the Civil Engineering in Oceans IV*, ASCE, New York, 1992.
- Olagnon, M., Prevosto, M. & Joubert, P., Nonlinear Spectral Computation of the Dynamic Response of a Single Cylinder. *Journal of Offshore Mechanics and Arctic Engineering, ASME*, **110** (1988) 278–81.
- Zhao, J. & Kareem, A., Response Statistics of Tension Leg Platforms to Wind and Wave Loads: A Statistical Quadraticization Approach. *Proceedings of the International Conference on Structural Safety and Reliability*, Innsbruck, Austria, A. A. Balkema Publishers, Rotterdam, Netherlands (in press).
- McIver, D.B., Parametrically-Excited Oscillations in Offshore Structures. *Proceedings of BOSS Conference*, Trondheim, Norway, Vol. 2, 1976.
- Rainey, R.C.T., The Dynamics of Tethered Platforms. *Trans. Royal Institute of Naval Architects*, **120** (1977) 50–80.
- Li, Y. & Kareem, A., Computation of Wave-Induced Drift Forces Introduced by Displaced Position of Compliant Offshore Platforms. *Journal of Offshore Mechanics and Arctic Engineering, ASME*, **114** (1992) 175–84.
- Spanos, P.D. & Argarwal, V.K., Response of a Simple Tension Leg Platform Model to Wave Forces Calculated at the Displaced Position. *ASME, Journal of Energy Resources Technology*, **106** (1984) 437–43.
- Pinkster, J.A., Mean and Low Frequency Wave Drifting Forces on Floating Structures. *Ocean Engineering*, **6** (1979) 593–615.
- Newman, J.N., Second Order Slowly Varying Forces, Irregular Waves. *Proceedings International Symposium on Dynamics of Marine Vehicles and Offshore Structures in Waves*, University College, London, 1974.
- Spanos & Donley, Stochastic Response of a Tension Leg Platform to Viscous Drift Forces, *Proceedings of the 9th OMAE Conference*, ASME, Houston, TX, 1990.
- Mo, O. & Moan, T., Environmental Load Effects Analysis of Guyed Towers. *Journal of Energy Resources Technology, ASME*, **107** (1985) 24–33.
- Li, Y. & Kareem, A., A Description of Hydrodynamic Forces on Tension Leg Platform Using a Multivariate Hermite Expansion. *Proceedings of the Offshore Mechanics & Arctic Engineering*, ASME, Houston, 1990.
- Li, Y. & Kareem, A., Simulation of Multivariate Stationary and Nonstationary Random Processes: A Recent Development. *Computational Stochastic Mechanics*, P.D. Spanos and C.A. Brebbia. Elsevier Applied Sciences, 1991.
- Shinozuka, M., Monte Carlo Solution of Structural Dynamics, *Computer & Structures*, **2** (1972) 855–74.
- Spanos, P.D. & Mignolet, M.P., Z-Transform Modelling of P-M Wave Spectrum. *Journal of Engineering Mechanics*, **112** (1986) 745–59.
- Li, Y. & Kareem, A., Parametric Modelling of Stochastic Wave Effects on Offshore Platforms. *Applied Ocean Research* (in press).
- Borgman, L.E., Directional Spectral Density of Forces on Fixed Platforms. *Proc. Directional Wave Spectra Applications*, Berkeley, California, 1981.
- Brigham, E.O., *The Fast Fourier Transform*. Prentice-Hall, Inc., New Jersey, 1974.
- Spidsoc, N. & Sigbjornsson, R., On the Reliability of Standard Wave Spectra in Structural Response Analysis. *Eng. Struc.*, **2** (1980) 123–25.
- Bendat, J.S. & Piersol, A.G., *Random Data: Analysis and Measurement Procedures*. Wiley-Interscience, NY, 1971.

Appendix A: Formulation of the Quadratic Transfer Function by the Boundary Element Method

Here we introduce a comparatively simple algorithm for the computation of the potential drift forces on a TLP type structure. The computation is based on the boundary element method. A minor modification of

an existing computer program for the first-order wave diffraction and radiation loads leads to the program for the drift force computation. Considering that the drift force is concentrated near the water surface level, the contribution of the pontoons to the drift force is neglected. This leads to a simplified configuration of the TLP with vertical cylindrical columns.

Let a cylindrical coordinate system $0r\theta\zeta$ be established with respect to a cylinder (see Fig. A-1). The water particle velocity vector $\mathbf{u}(t, \mathbf{r})$ (i.e. $\nabla\phi(t, \mathbf{r})$) can be expressed for \mathbf{r} located on the curved surface of the cylinder,

$$\mathbf{u}(t, \mathbf{r}) = u_\theta(t, \mathbf{r})\mathbf{e}_\theta + u_\zeta(t, \mathbf{r})\mathbf{e}_\zeta$$

and if point \mathbf{r} is on the cylinder bottom,

$$\mathbf{u}(t, \mathbf{r}) = u_\theta(t, \mathbf{r})\mathbf{e}_\theta + u_r(t, \mathbf{r})\mathbf{e}_r \quad (\text{A1})$$

where \mathbf{e}_r , \mathbf{e}_θ and \mathbf{e}_ζ denote unit vectors. For symbolic simplicity, $u_{r\zeta}(t, \mathbf{r})$ is introduced, which represents $u_\alpha(t, \mathbf{r})$ if the point \mathbf{r} is on the lateral surface and $u_r(t, \mathbf{r})$ if \mathbf{r} is at the cylinder bottom. Then, eqn (1) is given by

$$\begin{aligned} \mathbf{F}_{\text{pot}}(t) = & \int_{A_0} \frac{1}{2} \rho [u_\theta^2(t, \mathbf{r}) + u_{r\zeta}^2(t, \mathbf{r})] \mathbf{T}(\mathbf{r}) dA \\ & - \int_{WL} \frac{1}{2} \rho g \eta^2(t, \mathbf{r}) \mathbf{T}(\mathbf{r}) d\eta \end{aligned} \quad (\text{A2})$$

The water particle velocities and disturbed wave surface for bi-chromatic wave of unit amplitude at frequencies f_n and f_m are given by

$$\begin{aligned} u_\theta(t, \mathbf{r}) & \stackrel{\text{Re}}{=} u_\theta(f_n, \mathbf{r}) \exp [j(2\pi f_n t + \epsilon_n)] \\ & + u_\theta(f_m, \mathbf{r}) \exp [j(2\pi f_m t + \epsilon_m)] \\ u_{r\zeta}(t, \mathbf{r}) & \stackrel{\text{Re}}{=} u_{r\zeta}(f_n, \mathbf{r}) \exp [j(2\pi f_n t + \epsilon_n)] \\ & + u_{r\zeta}(f_m, \mathbf{r}) \exp [j(2\pi f_m t + \epsilon_m)] \\ \eta(t, \mathbf{r}) & \stackrel{\text{Re}}{=} \eta(f_n, \mathbf{r}) \exp [j(2\pi f_n t + \epsilon_n)] \\ & + \eta(f_m, \mathbf{r}) \exp [j(2\pi f_m t + \epsilon_m)] \end{aligned} \quad (\text{A3})$$

where $u_\theta(f_n, \mathbf{r})$, $u_{r\zeta}(f_n, \mathbf{r})$ and $\eta(f_n, \mathbf{r})$ denote the complex amplitudes of the water particle velocities and disturbed wave surface elevation corresponding to the incident wave at frequency f_n . Substituting eqns (A3) and eqn (A2) and following eqn (4), the quadratic transfer function is reduced to

$$\begin{aligned} \mathbf{H}_{\text{pot}}(f_n, f_m) = & \int_{A_0} \frac{1}{4} \rho [u_\theta(f_n, \mathbf{r}) u_\theta^*(f_m, \mathbf{r}) \\ & + u_{r\zeta}(f_n, \mathbf{r}) u_{r\zeta}^*(f_m, \mathbf{r})] \mathbf{T}(\mathbf{r}) dA \\ & - \int_{WL} \frac{1}{4} \rho g [\eta(f_n, \mathbf{r}) \eta^*(f_m, \mathbf{r})] \mathbf{T}(\mathbf{r}) dL \end{aligned} \quad (\text{A4})$$

The remaining task is to express the complex functions $u_\theta(f_n, \mathbf{r})$, $u_{r\zeta}(f_n, \mathbf{r})$ and $\eta(f_n, \mathbf{r})$ in terms of the incident wave surface elevation $\eta(f_n)$ with unit

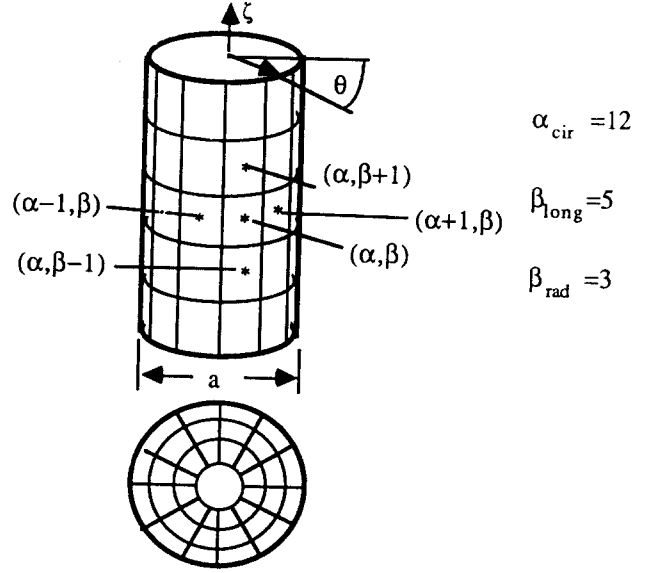


Fig. A1. Discretization of a cylinder surface for potential drift force computation.

amplitude. Let the lateral surface of each cylinder be discretized into $\alpha_{\text{cir}} \times \beta_{\text{long}}$ elements, the bottom being discretized into $(\alpha_{\text{cir}} \times \beta_{\text{rad}} + 1)$ elements and each element be identified by $\alpha\beta$ (see Fig. A1). The complex velocity potential $\Phi(f_n, \mathbf{r}_{\alpha\beta})$ at the center of element $\alpha\beta$ corresponding to the unit amplitude wave surface elevation can be computed by the boundary element method (Kareem & Li⁹).

The facets located on the same circle form a closed loop. It is expected that $u_\theta(f_n, \mathbf{r})$ is continuous along the circumference. This requirement can be satisfied by the central difference method, which allows $u_\theta(f_n, \mathbf{r})$ at the center of the element number $\alpha\beta$ be given by

$$u_\theta(f_n, \mathbf{r}_{\alpha\beta}) = \frac{\Phi[f_n, \mathbf{r}_{(\alpha+1)\beta}] - \Phi[f_n, \mathbf{r}_{(\alpha-1)\beta}]}{2r \frac{2\pi}{\alpha_{\text{cir}}}} \quad (\text{A5})$$

The longitudinal or radial velocities, $u_{r\zeta}(f_n, \mathbf{r})$, at the last facet near the end cannot be computed by the central difference method. Hence, a polynomial interpolation is introduced:

$$\Phi \left[f_n, \left(\theta_\alpha, \frac{a}{2}, \zeta \right) \right] = \sum_{\beta=1}^{\beta_{\text{long}}} \sum_{\substack{\gamma=1 \\ \gamma \neq \beta}}^{\beta_{\text{long}}} \left(\frac{\zeta - \zeta_\gamma}{\zeta_\beta - \zeta_\gamma} \right) \Phi(f_n, \mathbf{r}_{\alpha\beta}) \quad (\text{A6})$$

This allows the potential at zero depth (i.e. at the mean water level) to be interpolated for the computation of the disturbed water surface elevation $\eta(f_n, \mathbf{r})$. The differentiation of eqn (A1) leads to the water particle velocity $u_{r\zeta}(f_n, \mathbf{r})$.

Finally, substituting $u_\theta(f_n, \mathbf{r})$, $u_\theta(f_m, \mathbf{r})$, $u_{r\zeta}(f_m, \mathbf{r})$, $u_{r\zeta}(f_n, \mathbf{r})$, $\eta(f_n, \mathbf{r})$ and $\eta(f_m, \mathbf{r})$ in eqn (A4) yields the required vector of quadratic transfer functions $\mathbf{H}_{\text{pot}}(f_n, f_m)$.